

---

# CP-Guard+: A New Paradigm for Malicious Agent Detection and Defense in Collaborative Perception

---

Senkang Hu<sup>1\*</sup> Yihang Tao<sup>1\*</sup> Zihan Fang<sup>1</sup> Guowen Xu<sup>2</sup> Yiqin Deng<sup>1</sup> Sam Kwong<sup>3</sup> Yuguang Fang<sup>1</sup>

## Abstract

Collaborative perception (CP) is a promising method for safe connected and autonomous driving, which enables multiple vehicles to share sensing information to enhance perception performance. However, compared with single-vehicle perception, the openness of a CP system makes it more vulnerable to malicious attacks that can inject malicious information to mislead the perception of an ego vehicle, resulting in severe risks for safe driving. To mitigate such vulnerability, we first propose a new paradigm for malicious agent detection that effectively identifies malicious agents at the feature level without requiring verification of final perception results, significantly reducing computational overhead. Building on this paradigm, we introduce CP-GuardBench, the first comprehensive dataset provided to train and evaluate various malicious agent detection methods for CP systems. Furthermore, we develop a robust defense method called CP-Guard+, which enhances the margin between the representations of benign and malicious features through a carefully designed Dual-Centered Contrastive Loss (DCCLoss). Finally, we conduct extensive experiments on both CP-GuardBench and V2X-Sim, and demonstrate the superiority of CP-Guard+.

## 1. Introduction

The development of collaborative perception (CP) has been driven by the increasing demand for accurate and reliable perception in autonomous driving systems (Chen et al., 2019b;a; Li et al., 2022; Hu et al., 2024f; 2023; 2024b; Fang et al., 2024a; Xu et al., 2022; Hu et al., 2024d;e;a; Tao et al., 2025; Lin et al., 2024c;b). Single-agent perception systems,

which rely solely on the onboard sensors of a single vehicle, are restricted by limited sensing range and occlusion. On the contrary, CP systems incorporate multiple connected and autonomous vehicles (CAVs) to collaboratively capture their surrounding environments. Specifically, CAVs in a CP system can be divided into two categories: the ego CAV and helping CAVs. The helping CAVs send complementary sensing information (most methods send intermediate features) to the ego CAV, and the ego CAV then leverages this complementary information to enhance its perception performance (Balkus et al., 2022; Han et al., 2023; Hu et al., 2024c; Wang et al., 2020; Fang et al., 2025; 2024b; Tao et al., 2024; Fang et al., 2024c; Lin et al., 2024f;a;d). For example, the ego CAV can detect occluded objects and extend the sensing range after fusing the received information.

Despite many advantages of CP outlined above, it also has several crucial drawbacks. Compared to single-agent perception systems, CP is more vulnerable to security threats and easier attack since it requires receiving and fusing information from other CAVs, which expands the attack surface. In particular, malicious agents can directly send intermediate features with adversarial perturbations to fool the ego CAV or a man-in-the-middle who can capture the intermediate feature maps and manipulate them. Figure 1a illustrates the vulnerability of CP to malicious agents. In addition, several attack methods have been designed to fool CP. For example, Tu *et al.* (Tu et al., 2021) developed a method to generate indistinguishable adversarial perturbations to attack the multi-agent communication in CP, which can severely degrade the perception performance (Lin et al., 2024e; 2025; 2023).

The inability for the ego CAV to accurately detect and eliminate malicious agents from its collaboration network poses significant risks to CP, potentially resulting in compromised perception outcomes and catastrophic consequences. For instance, the ego CAV might misinterpret traffic light statuses or fail to detect objects ahead of the road, resulting in severe traffic accidents or even fatalities. Hence, it is crucial to develop a defense mechanism for CP that is resilient to attacks from malicious agents and capable of eliminating them from its collaboration network.

To address the security threats in CP, some previous works

---

\*Equal contribution <sup>1</sup>Department of Computer Science, City University of Hong Kong. <sup>2</sup>School of Computer Science and Engineering, University of Electronic Science and Technology of China. <sup>3</sup>Department of Computing and Decision Sciences, Lingnan University.. Correspondence to: Yuguang Fang <my.Fang@cityu.edu.hk>.

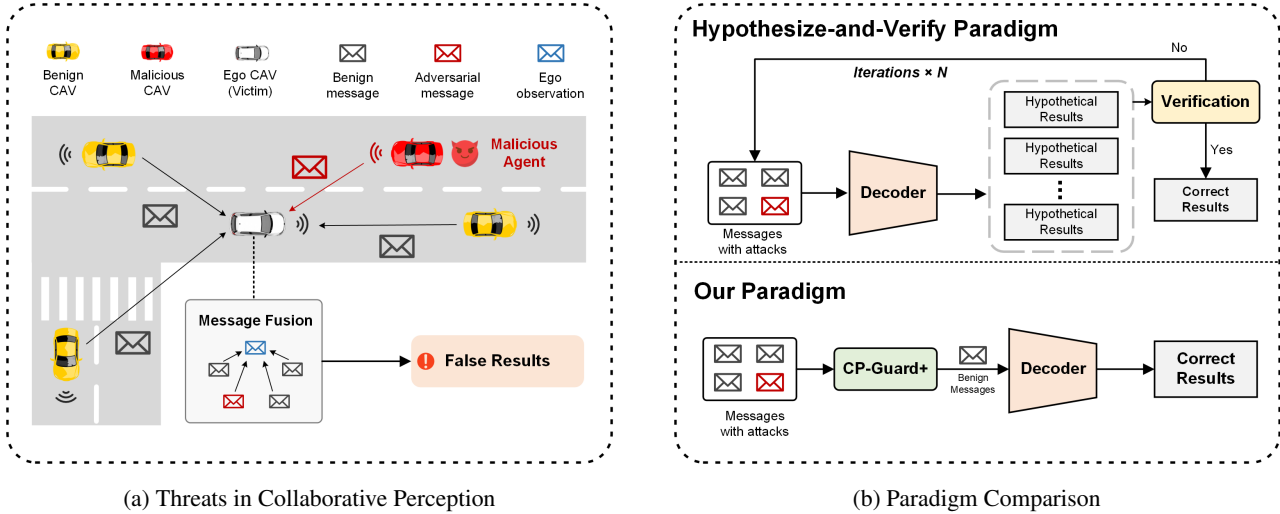


Figure 1. (a) **Illustration of the threats of malicious agent in collaborative perception.** Malicious CAVs could send intricately crafted adversarial messages to an ego CAV, which will mislead it to generate false positive perception outputs. (b) **Comparison between the proposed CP-Guard+ with the traditional hypothesize-and-verify malicious agent detection methods.** Hypothesize-and-verify involves multiple rounds of malicious agent detection iterations at the output level and requires the generation of multiple hypothetical outputs for verification, incurring high computational overhead. In contrast, CP-Guard+ directly outputs robust CP results with intermediate feature-level detection, significantly reducing the computational overhead.

have investigated the defense mechanisms against malicious agents. For example, Li *et al.* (Li *et al.*, 2023) leveraged random sample consensus (RANSAC) to sample a subset of collaborators and calculate the intersection of union (IoU) of the bounding boxes to verify whether there is any malicious agent among the collaboration network. Zhao *et al.* (Zhao *et al.*, 2024) designed a match loss and a reconstruction loss as statistics to measure the consensus between the ego CAV and the collaborators. However, these methods all follow a hypothesize-and-verify paradigm, which requires generating multiple hypothetical perception results and verifying the consistency between the ego CAV and the collaborators. This approach is computation-intensive and time-consuming, which hinders its scalability, leading to the following question:

*Is it feasible to detect malicious agents directly at the feature level?*

As illustrated in Figure 1b, the new paradigm shifts the focus to feature-level detection, eliminating the need to generate multiple hypothetical perception results. This direct approach can significantly reduce computational overhead, thereby enhancing the efficiency of malicious agent detection in CP systems.

Although this idea is concise and appealing, there are still some challenges in realizing it. Firstly, to detect malicious agents at the feature level, we need to train a deep neural network (DNN) model on a large-scale dataset to help it learn the features of benign and malicious agents. However, there is a lack of a benchmark dataset for feature-level mali-

cious agent detection in CP systems. The existing datasets for CP, such as V2X-Sim (Li *et al.*, 2022) and OPV2V (Xu *et al.*, 2022), contain only benign agents and do not include malicious agents. Therefore, it is difficult to train a robust DNN model for malicious agent detection in CP systems without a well-annotated dataset. Secondly, in CP scenarios, the environments are highly dynamic and complex, making it unrealizable to directly use a classifier to categorize the received intermediate features for detecting malicious agents. This is because dynamic environments will cause a high false-positive rate (FPR). Additionally, adversarial perturbations are indistinguishable at the feature level, and the feature distributions of malicious agents and benign agents are highly similar. These factors make it difficult to train a robust model to distinguish malicious agents from benign agents.

To address the aforementioned challenges, we first generate a new dataset, CP-GuardBench, which is the first dataset for malicious agent detection in CP systems. Then, we propose CP-Guard+, a robust malicious agent detection method for CP systems. CP-Guard+ can effectively detect malicious agents at the feature level without verifying the final perception results, significantly reducing computational overhead and improving defense efficiency. Moreover, we design a Dual-Centered Contrastive Loss (DCCLoss) to tackle indistinguishability issues at feature level and further enhance robustness.

In summary, we investigate the malicious agent detection problem in CP systems and propose a new paradigm, namely, feature-level malicious agent detection. Addition-

ally, we construct CP-GuardBench, the first benchmark for malicious agent detection in CP systems. Furthermore, we propose CP-Guard+, a robust malicious agent detection framework with high robustness and computational efficiency. Finally, we conduct extensive experiments on CP-GuardBench and V2X-Sim, and demonstrate the superiority of our CP-Guard+.

## 2. Preliminaries

### 2.1. Formulation of Collaborative Perception

In this section, we formulate collaborative perception and give the pipeline of our CP system. Specifically, let  $\mathcal{X}^N$  denote the set of  $N$  CAVs in the CP system. CAVs in  $\mathcal{X}$  can be divided into two categories: the ego CAV and helping CAVs. The ego CAV is the one that needs to perceive its surrounding environment, while helping CAVs are the ones that send their complementary sensing information to the ego CAV to help it enhance its perception performance. Thus, each CAV can be an ego one and helping one, depending on its role in a perception process. We assume that each CAV is equipped with a feature encoder  $f_{\text{encoder}}(\cdot)$ , a feature aggregator  $f_{\text{agg}}(\cdot)$ , and a feature decoder  $f_{\text{decoder}}(\cdot)$ . For the  $i$ -th CAV in the set  $\mathcal{X}$ , the raw observation is denoted as  $\mathbf{O}_i$  (such as camera images and LiDAR point clouds), and the final perception results are denoted as  $\mathbf{Y}_i$ . The CP pipeline of the  $i$ -th CAV can be described as follows.

1. *Observation Encoding*: Each CAV encodes its raw observation  $\mathbf{O}_j$  into an initial feature map  $\mathbf{F}_j = f_{\text{encoder}}(\mathbf{O}_j)$ , where  $j \in \mathcal{X}^N$ .
2. *Intermediate Feature Transmission*: Helping CAVs transmit their intermediate features to the ego CAV:  $\mathbf{F}_{j \rightarrow i} = \mathbf{\Gamma}_{j \rightarrow i}(\mathbf{F}_j)$ ,  $j \in \mathcal{X}^N, j \neq i$ , where  $\mathbf{\Gamma}_{j \rightarrow i}(\cdot)$  denotes a transmitter that conveys the  $j$ -th CAV's intermediate feature  $\mathbf{F}_j$  to the ego CAV, while performing a spatial transformation.  $\mathbf{F}_{j \rightarrow i}$  is the spatially aligned feature in the  $i$ -th CAV's coordinate.
3. *Feature Aggregation*: The ego CAV receives all the intermediate features and fuses them into a unified observational feature  $\mathbf{F}_{\text{fused}} = f_{\text{agg}}(\mathbf{F}_{0 \rightarrow i}, \{\mathbf{F}_{j \rightarrow i}\}_{j \neq i, j \in \mathcal{X}^N})$ .
4. *Perception Decoding*: Finally, the ego CAV decodes the unified observational feature  $\mathbf{F}_{\text{fused}}$  into the final perception results  $\mathbf{Y} = f_{\text{decoder}}(\mathbf{F}_{\text{fused}})$ .

### 2.2. Adversarial Threat Model

Our focus is on the operation of an intermediate-fusion collaboration scheme, where an attacker introduces designed adversarial perturbations into the intermediate features to mislead the perception of the ego CAV. Since an attacker participates in the collaborative system with local perception model installation, we assume they have white-box access to

the model parameters. The attack procedure in each frame follows four sequential phases.

1. *Local Perception Phase*: All agents, including the malicious one, process their sensing data independently and extract intermediate features using feature encoders.

$$\mathbf{F}_k = f_{\text{encoder}}(\mathbf{O}_k), \quad k \in \mathcal{X}^N \quad (1)$$

This phase operates in parallel without inter-agent communication.

2. *Feature Communication Phase*: All agents broadcast their extracted features through the network. Malicious agent  $k$  collects feature information  $\{\mathbf{F}_{j \rightarrow i}\}$  from other agents. Feature-level transmission ensures minimal communication overhead compared to raw sensor data exchange.
3. *Attack Generation Phase*: A malicious agent executes the attack by first perturbing its local features and then propagating them through the collaborative perception pipeline described in Section 2.1. The attacker aims to optimize the perturbation  $\delta$  through an iterative process. The optimization objective is formulated as:

$$\arg \max_{\delta} \mathcal{L}(\mathbf{Y}^{\delta}, \mathbf{Y}^{\text{gt}}), \quad \text{s.t.} \quad \|\delta\| \leq \Delta \quad (2)$$

where  $\Delta$  bounds the perturbation magnitude to maintain attack stealthiness. The total loss function is designed to aggregate adversarial losses over all object proposals, targeting both classification and localization aspects:

$$\mathcal{L}(\mathbf{Y}^{\delta}, \mathbf{Y}^{\text{gt}}) = \sum_{p \in \mathbf{Y}^{\delta}} \mathcal{L}_{\text{adv}}(p, p^{\text{gt}}) \quad (3)$$

For each proposal  $p$  with the highest confidence class  $c = \arg \max\{p_i\}$ , we leverage a class-specific adversarial loss following (Tu et al., 2021):

$$\mathcal{L}_{\text{adv}}(p', p) = \begin{cases} -\log(1 - p'_c) \cdot \eta & c \neq k, p_c > \tau_1 \\ -\lambda p'_c \log(1 - p'_c) & c = k, p_c > \tau_2 \\ 0 & \text{otherwise} \end{cases}$$

where  $\eta$  represents the IoU between perturbed and original proposals to consider spatial accuracy,  $\tau_1$  and  $\tau_2$  are confidence thresholds for different attack scenarios,  $\lambda$  balances the importance of different attack objectives, and  $k$  denotes the background class.

4. *Defense and Final Perception Phase*: The ego vehicle integrates all received feature information, including potentially corrupted ones, to complete the final object detection task. Note that we focus exclusively on CP-specific vulnerabilities, excluding physical sensor attacks (e.g., LiDAR or GPS spoofing), which are general threats to CAVs. We also assume communication channels are secured with proper cryptographic protection.

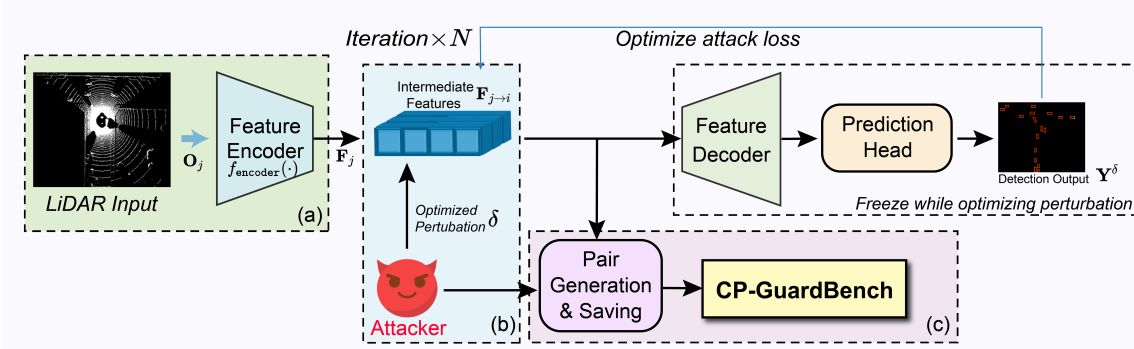


Figure 2. **Automatic Data Generation and Annotation Pipeline.** We first train a robust LiDAR collaborative object detector. Then, we discard the detection head and decoder and only keep the backbone as the intermediate feature generator. The data generation pipeline is shown in (a), (b), and (c), where (a) is the intermediate feature generation, (b) is the attack implementation, and (c) is the pair generation and saving.

### 3. CP-GuardBench

To facilitate feature-level malicious agent detection in CP systems, we propose to develop CP-GuardBench, the first benchmark for malicious agent detection in CP systems. It provides a comprehensive dataset for training and evaluating malicious agent detection methods. In this section, we will introduce the details of CP-GuardBench, including the automatic data generation and annotation pipeline in Section 3.1, and the data visualization and statistics in Section 3.2.

#### 3.1. Automatic Data Generation and Annotation

We build CP-GuardBench based on one of the most widely used datasets in the CP field, V2X-Sim (Li et al., 2022), which is a comprehensive simulated multi-agent perception dataset for V2X-aided autonomous driving. In this section, we introduce the automatic data generation and annotation pipeline of CP-GuardBench. The pipeline is shown in Figure 2. It consists of three steps: 1) intermediate feature generation, 2) attack implementation, and 3) pair generation and saving.

Specifically, we first train a robust LiDAR collaborative object detector, which consists of a convolutional backbone, a convolutional decoder, and a prediction head for classification and regression (Luo et al., 2018). As for the fusion method, we adopt the mean fusion method to fuse the intermediate features from different collaborators. Subsequently, the backbone is retained for extracting intermediate features, which are then transmitted and utilized by an ego CAV as supplementary information.

Secondly, the attacks are implemented and applied to the intermediate features. The detection head and decoder are then frozen to generate the attacked detection results and optimize the adversarial perturbations. As shown in Figure 2, several iterations are required to optimize the perturbations, and the loss function differs for different attack types. In our CP-GuardBench, we consider five types of attacks,

including Projected Gradient Descent (PGD) (Madry et al., 2018), Carini & Wagner (C&W) attack (Carlini & Wagner, 2017), Basic Iterative Method (BIM) (Kurakin et al., 2017), Gaussian Noise Perturbation (GN), and Fast Gradient Sign Method (FGSM) (Goodfellow et al., 2015). The implementation details can be found in Appendix ??.

In the generation of attack data, we randomly choose one of the attacks mentioned above and generate the corresponding attack data in each iteration. Finally, the perturbed features will be annotated with the corresponding attack type and saved for later use.

#### 3.2. Data Visualization and Statistics

We visualize the samples of the generated data in Figures 3(a), (b), (c), and (d). We observe that attacks are so stealthy that it is very hard to see the difference with the naked eye, which poses a great challenge to address the detection of malicious agents.

To construct CP-GuardBench, we randomly sample 9000 frames from V2X-Sim and generate 42200 feature-label pairs. The data is then split into training, validation, and test sets with a ratio of 8:1:1. The data statistics are shown in Figures 3(e), (f), and (g). Figure 3(e) illustrates the distribution of the number of collaborators, which is the number of agents that collaboratively perceive environments. The number of collaborators ranges from 3 to 6, with the most common scenario being 4 collaborators, accounting for 46.0% of the total data. 5 and 6 collaborators are also common, accounting for 29.9% and 19.5% of the total data, respectively. Regarding the distribution of attack types, as depicted in Figure 3(f), we observe that the attack types are evenly distributed, with each type accounting for approximately 20% of the total data. This is due to the random selection of one attack type in each iteration. Figure 3(g) illustrates the attack ratio, which represents the ratio of the number of attackers to the total number of agents in a collaboration network. The maximum attack ratio exceeds 0.3,

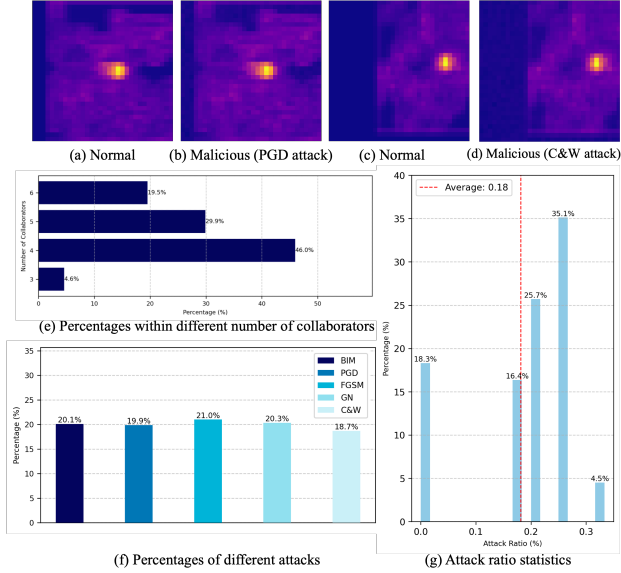


Figure 3. Visualization and Statistics of CP-GuardBench. (a), (b), (c) and (d) are visualization, which visualize the normal intermediate features and the adversarial examples perturbed by different malicious agents. We can see the adversarial examples are almost identical to the normal examples, which indicates the challenges in detecting malicious agents. (e), (f), (g) and (h) are the statistics of CP-GuardBench, including the number of collaborators, attack ratio and attack types.

the minimum is 0, and the average attack ratio is 0.18.

## 4. CP-Guard+

In this section, we present our CP-Guard+, a tailored defense method for CP scenarios that effectively detects malicious agents. It consists of two techniques: 1) Residual Latent Feature Learning, which learns the residual features of benign and malicious agents, and 2) Dual Centered Contrastive Loss (DCCLoss), which clusters the representation of benign features into a compact space and ensures that the representation of malicious features is as distant from the benign space as possible.

### 4.1. Residual Latent Feature Learning

In CP scenarios, the dynamic environment causes noisy, non-stationary data distributions. Directly detecting malicious agents can be challenging due to this noise, as object detectors’ feature maps often mix foreground and background information.

To tackle this challenge, we propose to learn residual latent features instead of directly learning the features of benign or malicious agents. By focusing on the differences between the collaborators’ feature maps and the ego agent’s feature maps, the model can better distinguish between benign and malicious agents. This mechanism is also inspired by the idea that the collaborators’ intermediate feature maps will achieve a consensus rather than conflict with the ego CAV’s

intermediate feature maps.

Specifically, given the collaborators’ intermediate feature maps  $\{\mathbf{F}_{j \rightarrow i}\}_{j \neq i, j \in \mathcal{X}^N}$  and the ego CAV’s intermediate feature maps  $\mathbf{F}_i$ , the residual feature is obtained as:  $\mathbf{F}_{j \rightarrow i}^{\text{res}} = \mathbf{F}_i - \mathbf{F}_{j \rightarrow i}$ .

Then, we can leverage the residual latent features to detect malicious agents by modeling the detection problem as a binary classification task. A binary classifier  $f_{\text{cls}}(\mathbf{x}; \theta)$  is trained on the residual latent features to distinguish between benign (labeled 0) and malicious (labeled 1) agents. The model is optimized using the cross-entropy loss  $\mathcal{L}_{\text{CE}}$ :

$$\min_{\theta} \mathcal{L}_{\text{CE}}(f_{\text{cls}}(\mathbf{F}_{j \rightarrow i}^{\text{res}}; \theta), y_{j \rightarrow i}) \quad (4)$$

where  $y_{j \rightarrow i}$  is the ground truth label of residual feature  $\mathbf{F}_{j \rightarrow i}^{\text{res}}$ .

### 4.2. Dual-Centered Contrastive Loss

In practice, attackers can continuously design new attacks to manipulate the victim’s intermediate feature maps. Therefore, we need a model that is resistant to unseen attacks, which means the model should cluster the representation of benign features into a more compact space and ensure that the representation of malicious features is as distant from the benign space as possible.

To tackle this challenge, we propose a Dual-Centered Contrastive Loss (DCCLoss), which is a contrastive learning-based objective function. It explicitly models the distribution relationship between benign and malicious features, enhancing the positive pairs (features of the same class) to their corresponding center closer, thereby enhancing the internal consistency of both benign and malicious features. Meanwhile, negative pairs (features from different classes) will be pushed away from each other’s centers, ensuring maximal separation between benign and malicious features in the feature space. In this way, the robustness of the model against unseen attacks is improved.

Specifically, we first leverage the output of the penultimate fully connected layer  $f_{\text{cls}}$  to obtain the one-dimensional vector  $\{\mathcal{V}_i\}_{i=0,1,\dots,N-1}$  of residual features  $\{\mathbf{F}_{j \rightarrow i}^{\text{res}}\}_{j \neq i, j \in \mathcal{X}^N}$ . Then, we introduce two feature centers in DCCLoss:

1. Benign feature center ( $\mathbf{c}_b$ ): represents the center of all benign features, ensuring a compact distribution of benign features.
2. Malicious feature center ( $\mathbf{c}_{\text{mal}}$ ): represents the center of all malicious features, ensuring maximal separation between malicious and benign feature distributions.

The benign feature center  $\mathbf{c}_b$  and the malicious feature center  $\mathbf{c}_{\text{mal}}$  are computed by averaging the vectors of benign and malicious features, respectively:

**Table 1. Performance Evaluation of CP-Guard+ on CP-GuardBench.** We report the average accuracy, true positive rate (TPR), false positive rate (FPR), precision, and F1 score of CP-Guard+ on CP-GuardBench with different attack methods and perturbation budgets  $\Delta = 0.10, 0.25, 0.5, 0.75$ .

Metrics	$\Delta = 0.10$					$\Delta = 0.25$				
	Accuracy $\uparrow$	TPR $\uparrow$	FPR $\downarrow$	Precision $\uparrow$	F1 Score $\uparrow$	Accuracy $\uparrow$	TPR $\uparrow$	FPR $\downarrow$	Precision $\uparrow$	F1 Score $\uparrow$
PGD	99.79	98.97	0.00	100.00	99.48	99.93	100.00	0.09	99.66	99.83
BIM	99.93	100.00	0.09	99.66	99.83	100.00	100.00	0.00	100.00	100.00
C&W	99.73	98.96	0.09	99.65	99.30	99.86	100.00	0.17	99.32	99.66
FGSM	91.23	56.80	0.09	99.40	72.29	98.77	94.24	0.09	99.64	96.86
GN	91.02	55.63	0.09	99.39	71.33	98.49	92.88	0.09	99.64	96.14
Average	96.34	82.07	0.07	99.62	88.45	99.41	97.42	0.09	99.65	98.50

Metrics	$\Delta = 0.50$					$\Delta = 0.75$				
	Accuracy $\uparrow$	TPR $\uparrow$	FPR $\downarrow$	Precision $\uparrow$	F1 Score $\uparrow$	Accuracy $\uparrow$	TPR $\uparrow$	FPR $\downarrow$	Precision $\uparrow$	F1 Score $\uparrow$
PGD	99.86	100.00	0.17	99.32	99.66	99.86	100.00	0.17	99.33	99.66
BIM	99.93	100.00	0.09	99.66	99.83	99.93	100.00	0.09	99.66	99.83
C&W	99.86	100.00	0.17	99.32	99.66	99.93	100.00	0.09	99.66	99.83
FGSM	99.93	100.00	0.09	99.66	99.83	99.79	99.66	0.17	99.32	99.49
GN	99.86	100.00	0.17	99.32	99.66	99.79	99.65	0.17	99.31	99.48
Average	99.89	100.00	0.14	99.46	99.73	99.86	99.86	0.14	99.46	99.66

$$\mathbf{c}_b = \frac{1}{N_b} \sum_{\mathcal{V}_i \in \{\mathcal{V}_b\}} \mathcal{V}_i, \quad \mathbf{c}_{\text{mal}} = \frac{1}{N_{\text{mal}}} \sum_{\mathcal{V}_i \in \{\mathcal{V}_{\text{mal}}\}} \mathcal{V}_i. \quad (5)$$

where  $N_b$  and  $N_{\text{mal}}$  are the numbers of benign and malicious vectors, respectively, and  $\mathcal{V}_b$  and  $\mathcal{V}_{\text{mal}}$  are the sets of benign and malicious vectors, respectively.

Moreover, denote  $(\mathcal{V}_m, \mathcal{V}_n)$  as a pair of features, which is a positive pair if they are from the same class (both benign or malicious) and a negative pair otherwise. We have the DCCLoss of one feature pair  $\ell(\mathcal{V}_m, \mathcal{V}_n)$  as:

$$\ell(\mathcal{V}_m, \mathcal{V}_n) = -\log \frac{\exp((\mathcal{V}_m - \mathbf{c}^{(m)}) \odot (\mathcal{V}_n - \mathbf{c}^{(n)})/\tau)}{\sum_{o=1, o \neq m}^N \mathbb{I} \cdot \exp((\mathcal{V}_m - \mathbf{c}^{(m)}) \odot (\mathcal{V}_o - \mathbf{c}^{(o)})/\tau)}, \quad (6)$$

$$\text{where } \mathcal{V}_x - \mathbf{c}^{(x)} = \begin{cases} \mathcal{V}_x - \mathbf{c}_b, & \text{if } \mathcal{V}_x \in \{\mathcal{V}_b\}, \\ \mathcal{V}_x - \mathbf{c}_{\text{mal}}, & \text{if } \mathcal{V}_x \in \{\mathcal{V}_{\text{mal}}\}, \end{cases}$$

where  $\mathbb{I}(\mathcal{V}_m, \mathcal{V}_o)$  is an indicator function that returns one or zero for positive or negative pairs, respectively.  $\tau$  is a temperature parameter and  $\odot$  denotes the cosine similarity, where  $\mathcal{V}_m \odot \mathcal{V}_n = \frac{\mathcal{V}_m^\top \mathcal{V}_n}{\|\mathcal{V}_m\| \|\mathcal{V}_n\|}$ . The final DCCLoss is the average of  $\ell$  of all positive pairs.

$$\mathcal{L}_{\text{DCCLoss}} = \sum_{m=1}^N \sum_{n=m+1}^N \frac{(1 - \mathbb{I}(\mathcal{V}_m, \mathcal{V}_n)) \ell(\mathcal{V}_m, \mathcal{V}_n)}{C(N, 2)}, \quad (7)$$

where  $C(N, 2) = \binom{N}{2} = N!/(2!(N-2)!)$ . During training, we use the combination of cross entropy loss and Eq. 7 to optimize the model:

$$\mathcal{L} = \mathcal{L}_{\text{CE}} + \alpha \cdot \mathcal{L}_{\text{DCCLoss}} \quad (8)$$

where  $\alpha$  is a hyperparameter to balance the two losses.

**Discussion of DCCLoss.** In so doing, the first term  $\mathcal{L}_{\text{CE}}$  quantifies the difference between the true distribution and the predicted distribution from the model, thereby penalizing the confidence in wrong predictions. The second term  $\mathcal{L}_{\text{DCCLoss}}$  contributes significantly to the learning process. Standard contrastive loss attempts to maximize the distance between negative pairs, which may cause the features of benign samples to gradually drift away from their center. However, DCCLoss calculates the distance using the feature center as a reference point, thus avoiding this issue. The optimization goal of DCCLoss is to maximize the angular distance between negative pairs to enhance feature discriminability while maintaining the compactness of benign sample features, keeping them as close to the feature center as possible. In other words, the introduction of dual-center modeling optimizes the distributional relationship between benign and malicious features, making them more separable and making the distributions of benign and malicious features more compact on its own, respectively. This helps resolve the distribution overlap problem and enhances the model’s ability to detect unseen attacks.

## 5. Experiments

### 5.1. Experimental Setup

**Dataset and Baselines.** In our experiments, we consider two datasets: CP-GuardBench and V2X-Sim (Li et al., 2022). We designate CAV #1 as the ego CAV and randomly select adversarial collaborators from the remaining CAVs. Additionally, we use ROBOSAC (Li et al., 2023) and MADE (Zhao et al., 2024) as baselines, which are two state-of-the-art CP defense methods based on the hypothesize-and-verify paradigm.

**Attack Settings.** We assess different CP defense meth-

Table 2. **Comparative results of CP-Guard+ on the V2X-Sim Dataset.** We report the AP@0.5 and AP@0.7 with different perturbation budgets  $\Delta$  and number of malicious agents  $N_{\text{mal}}$ .

Attack Method	Defense Method	$\Delta = 0.25, N_{\text{mal}} = 1$		$\Delta = 0.5, N_{\text{mal}} = 1$		$\Delta = 0.25, N_{\text{mal}} = 2$		$\Delta = 0.5, N_{\text{mal}} = 2$	
		AP@0.5	AP@0.7	AP@0.5	AP@0.7	AP@0.5	AP@0.7	AP@0.5	AP@0.7
PGD	No Defense	29.73	28.47	11.35	11.17	12.69	12.42	1.69	1.65
	MADE	64.63	45.22	64.81	44.89	62.45	43.49	63.04	43.77
	ROBOSAC	62.13	42.90	63.67	43.79	59.01	40.03	59.97	40.44
	CP-Guard+	<b>72.89</b>	<b>71.45</b>	<b>69.50</b>	<b>68.56</b>	<b>69.50</b>	<b>67.92</b>	<b>66.09</b>	<b>64.82</b>
C&W	No Defense	19.03	16.58	4.69	3.78	19.03	16.58	0.71	0.58
	MADE	65.26	45.24	<b>64.74</b>	45.65	63.41	44.28	<b>62.86</b>	42.93
	ROBOSAC	61.83	42.01	62.47	42.80	59.39	39.94	59.83	39.82
	CP-Guard+	<b>69.41</b>	<b>66.86</b>	60.64	<b>55.41</b>	<b>64.17</b>	<b>61.73</b>	58.54	<b>53.15</b>
BIM	No Defense	26.69	25.71	10.05	9.89	11.59	11.38	1.37	1.33
	MADE	66.11	45.94	65.51	45.47	64.36	43.89	63.56	44.09
	ROBOSAC	62.69	43.80	63.78	43.66	59.10	39.74	59.29	39.89
	CP-Guard+	<b>73.35</b>	<b>71.46</b>	<b>66.83</b>	<b>66.05</b>	<b>70.91</b>	<b>69.11</b>	<b>66.30</b>	<b>64.62</b>
Average	No Defense	25.15	23.59	8.70	8.28	14.44	13.46	1.27	1.19
	MADE	65.33	45.47	65.02	45.34	63.41	43.89	63.15	43.60
	ROBOSAC	62.21	42.90	63.31	43.42	59.37	39.90	59.70	40.05
	CP-Guard+	<b>71.88</b>	<b>69.92</b>	<b>65.66</b>	<b>63.34</b>	<b>68.19</b>	<b>66.25</b>	<b>63.64</b>	<b>60.86</b>
Upper-bound		79.94	78.40	79.94	78.40	79.94	78.40	79.94	78.40

ods targeted at five attacks: PGD attack (Madry et al., 2018), C&W attack (Carlini & Wagner, 2017), BIM attack (Kurakin et al., 2017), FGSM attack (Goodfellow et al., 2015), and GN attack. We set different perturbation sizes  $\Delta \in \{0.1, 0.25, 0.5, 0.75, 1.0\}$ . The number of malicious attackers varies in  $\{0, 1, 2\}$  and all the attackers are randomly assigned from the collaborators, where 0 attacker indicates an upper-bound case. For PGD, BIM and C&W attacks, the number of iteration steps is 15 and the step size is 0.1.

**Implementation Details.** The CP-Guard+ system is implemented using PyTorch, and we utilize the object detector described in Section 3.1. For each agent, the local LiDAR point cloud data is first encoded into  $32 \times 32$  bird’s eye view (BEV) feature maps with 256 channels prior to communication. For our CP-Guard+, we use ResNet-50 (He et al., 2016) as the backbone, and the training is performed for 50 epochs with batch size 10 and learning rate  $1 \times 10^{-3}$ . Our experiments are conducted on a server with four RTX A5000 GPUs. For mixed contrastive training, we utilize the output of the fully connected layers preceding the final output layer in the backbone to form a one-dimensional feature vector for each agent, the dimension of which is 2048.

**Evaluation Metrics.** We use a variety of metrics to evaluate the performance of our CP-Guard+ model. For malicious agent detection on our CP-GuardBench dataset, we consider Accuracy, True Positive Rate (TPR), False Positive Rate (FPR), Precision, and F1 Score. For CP defense on the V2X-Sim dataset, we use metrics including average precision (AP) at IoU=0.5 and IoU=0.7. Additionally, to assess the computation efficiency of different CP defense methods, we introduce the metric frames-per-second (FPS).

Table 3. **Generalization results of CP-Guard+.** Test perturbation budgets  $\Delta = 0.25$ .

Held-out	Accuracy	TPR	FPR	Precision	F1 Score
PGD	99.93	100.00	0.09	99.66	99.83
BIM	99.52	100.00	0.60	97.66	98.82
C&W	99.86	100.00	0.17	99.32	99.66
FGSM	95.82	79.66	0.09	99.58	88.51
GN	96.02	81.02	0.17	99.17	89.18
Average	98.23	92.94	0.22	99.08	95.20
Upper-bound	99.41	97.42	0.09	99.65	98.50

The definition of the metrics are provided in Table ?? in Appendix.

## 5.2. Quantitative Results

**Performance Evaluation of CP-Guard+.** We evaluated CP-Guard+ on the CP-GuardBench dataset using various attack methods and perturbation budgets ( $\Delta$ ), as detailed in Table 1. Metrics include Accuracy, True Positive Rate (TPR), False Positive Rate (FPR), Precision, and F1 Score. At  $\Delta = 0.25$ , CP-Guard+ achieved over 98% accuracy for PGD, BIM, and C&W attacks. FGSM and GN attacks showed lower accuracy, around 91.64% and 90.95%, due to their weaker impact unless perturbations are large. With  $\Delta = 0.5$ , the model maintained an average accuracy of 98.08% and a TPR of 97.07%. For  $\Delta = 0.75$  and  $\Delta = 1.0$ , accuracy was 98.43% and 98.53%, respectively. The model consistently showed high TPR and low FPR, indicating robust detection of true positives and minimal false positives. Overall, CP-Guard+ demonstrated strong performance and resilience across various attacks and perturbation levels.

**Performance Comparison with Other Defenses.** We com-

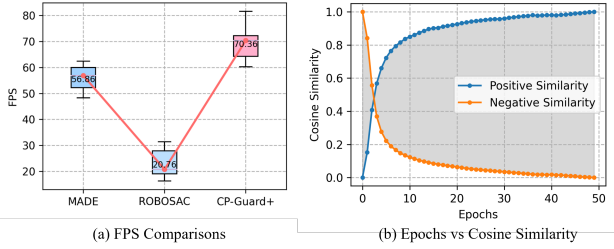


Figure 4. (a) FPS performance comparison between CP-Guard+ with and other baselines. (b) Cosine distance between the intermediate features of the malicious agent and the benign agent.

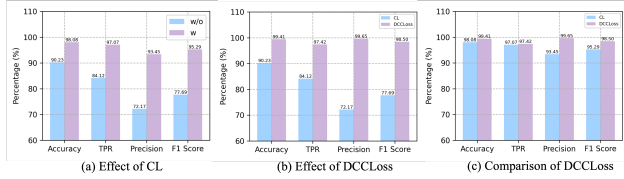


Figure 5. (a) Effectiveness of contrastive loss (CL). ‘w/o’ means without CL. ‘w/’ means with CL. (b) Effectiveness of DCCLoss. ‘w/o’ means without DCCLoss. ‘w/’ means with DCCLoss. (c) Comparison of DCCLoss.

pare CP-Guard+ with MADE (Zhao et al., 2024) and ROBOSAC (Li et al., 2023) on the V2X-Sim dataset. Table 2 shows that without defense, AP@0.5/0.7 significantly drops. CP-Guard+ consistently achieves the highest scores, even as the number of malicious agents or perturbation level increases. For  $\Delta = 0.25$  and  $N_{\text{mal}} = 1$ , CP-Guard+ achieves 71.88% AP@0.5 and 69.92% AP@0.7, outperforming the no-defense case by over 186% and 196%, respectively. It also surpasses MADE and ROBOSAC by notable margins. At  $\Delta = 0.5$  and  $N_{\text{mal}} = 2$ , CP-Guard+ maintains superior performance, confirming its robustness and superiority.

**FPS Comparison.** We compare the FPS performance of CP-Guard+ with MADE and ROBOSAC, as shown in Figure 4(a). The median FPS values for MADE, ROBOSAC, and CP-Guard+ are 56.86, 20.76, and 70.36, respectively. CP-Guard+ achieves a 23.74% higher FPS than MADE and a 238.92% increase over ROBOSAC, representing a significant improvement. These results highlight the high computational efficiency of our CP-Guard+.

**Generalization of CP-Guard+.** To evaluate our method’s generalization ability, we conducted experiments using a leave-one-out strategy. In this approach, we iteratively excluded one type of attack from the training set, trained the model on the remaining attacks, and then tested its performance on the held-out attack type. The experimental results are presented in Table 3. From the table, we can see that our method achieves strong generalization ability on unseen attacks. Compared to the upper-bound case, our method experiences only a little decrease in overall performance. These findings underscore our method’s robust capability to detect and handle unseen attack patterns.

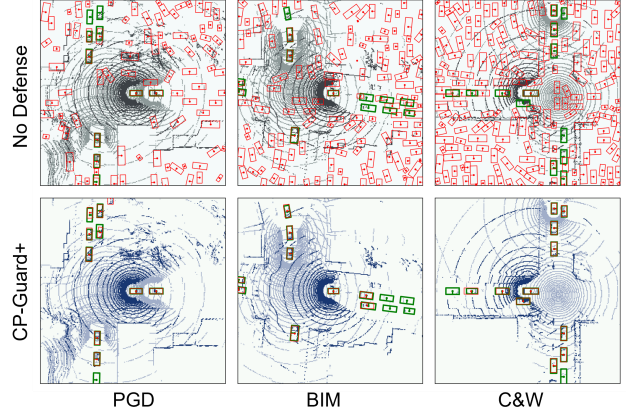


Figure 6. Visualization and Qualitative Results. We visualize the results of the CP systems with and without defense by CP-Guard+. The red bounding boxes represent the predicted outcomes, while the green ones denote the ground truth.

### 5.3. Ablation Study and Visualization

**The Effectiveness of DCCLoss.** We assess the impact of DCCLoss on CP-Guard+ performance. Figure 5 shows the effectiveness of DCCLoss and its superiority compared with contrastive loss (CL) (Chen et al., 2020). Figure 5(b) shows that this training significantly boosts performance, including Accuracy, TPR, Precision, and F1 score. Figure 5(c) shows the comparison results between DCCLoss and CL, which demonstrate that our DCCLoss outperforms CL and shows its effectiveness in malicious agent detection. In addition, Figure 4(b) illustrates that DCCLoss increases the cosine distance between negative pairs and decreases it between positive pairs, enhancing the model’s ability to distinguish between malicious and benign agents.

**Visualization.** Figure 6 visualizes the CP system’s results with and without the CP-Guard+ defense mechanism. The top row shows that without defense, malicious agents cause numerous false positives, compromising system performance and security. The bottom row demonstrates that CP-Guard+ effectively detects and eliminates malicious agents, reducing false positives and increasing the true positive rate, confirming its effectiveness.

## 6. Conclusion

In this paper, we have proposed a new paradigm for malicious agent detection in CP systems, which directly detects malicious agents at the feature level without generating multiple hypothetical results, significantly reducing system complexity and computation cost. We have also constructed a new benchmark, CP-GuardBench, for malicious agent detection in CP systems, which is the first benchmark in this field. Furthermore, we have developed CP-Guard+, a resilient framework for detecting malicious agents in CP systems, capable of identifying malicious agents at the feature level without the need to verify the final perception results,



significantly reducing the computation cost and increasing frame rate. We hope the new benchmark and the proposed framework CP-Guard+ can contribute to the community and promote further development of secure and reliable CP systems.

## References

- Balkus, S. V., Wang, H., Cornet, B. D., Mahabal, C., Ngo, H., and Fang, H. A Survey of Collaborative Machine Learning Using 5G Vehicular Communications. *IEEE Communications Surveys & Tutorials*, 24(2):1280–1303, 2022. ISSN 1553-877X. doi: 10.1109/COMST.2022.3149714.
- Carlini, N. and Wagner, D. Towards evaluating the robustness of neural networks, 2017.
- Chen, Q., Ma, X., Tang, S., Guo, J., Yang, Q., and Fu, S. F-cooper: Feature based cooperative perception for autonomous vehicle edge computing system using 3D point clouds. In *Proceedings of the 4th ACM/IEEE Symposium on Edge Computing*, pp. 88–100, Arlington Virginia, November 2019a. ACM. ISBN 978-1-4503-6733-2. doi: 10.1145/3318216.3363300.
- Chen, Q., Tang, S., Yang, Q., and Fu, S. Cooper: Cooperative Perception for Connected Autonomous Vehicles Based on 3D Point Clouds. In *2019 IEEE 39th International Conference on Distributed Computing Systems (ICDCS)*, pp. 514–524, Dallas, TX, USA, July 2019b. IEEE. ISBN 978-1-7281-2519-0. doi: 10.1109/ICDCS.2019.00058.
- Chen, T., Kornblith, S., Norouzi, M., and Hinton, G. A Simple Framework for Contrastive Learning of Visual Representations. In *Proceedings of the 37th International Conference on Machine Learning*, pp. 1597–1607. PMLR, November 2020.
- Fang, Z., Hu, S., An, H., Zhang, Y., Wang, J., Cao, H., Chen, X., and Fang, Y. PACP: Priority-Aware Collaborative Perception for Connected and Autonomous Vehicles. *IEEE Transactions on Mobile Computing*, 23(12):15003–15018, December 2024a. ISSN 1558-0660. doi: 10.1109/TMC.2024.3449371.
- Fang, Z., Hu, S., Yang, L., Deng, Y., Chen, X., and Fang, Y. PIB: Prioritized Information Bottleneck Framework for Collaborative Edge Video Analytics, 2024b.
- Fang, Z., Lin, Z., Hu, S., Cao, H., Deng, Y., Chen, X., and Fang, Y. IC3M: In-Car Multimodal Multi-object Monitoring for Abnormal Status of Both Driver and Passengers, 2024c.
- Fang, Z., Hu, S., Wang, J., Deng, Y., Chen, X., and Fang, Y. Prioritized information bottleneck theoretic framework with distributed online learning for edge video analytics. *IEEE Transactions on Networking*, pp. 1–17, 2025. doi: 10.1109/TON.2025.3526148.
- Goodfellow, I. J., Shlens, J., and Szegedy, C. Explaining and harnessing adversarial examples, 2015.
- Han, Y., Zhang, H., Li, H., Jin, Y., Lang, C., and Li, Y. Collaborative Perception in Autonomous Driving: Methods, Datasets and Challenges. *IEEE Intelligent Transportation Systems Magazine*, 15(6):131–151, November 2023. ISSN 1939-1390, 1941-1197. doi: 10.1109/MITS.2023.3298534.
- He, K., Zhang, X., Ren, S., and Sun, J. Deep Residual Learning for Image Recognition. In *2016 IEEE Conference on Computer Vision and Pattern Recognition (CVPR)*, pp. 770–778, Las Vegas, NV, USA, June 2016. IEEE. ISBN 978-1-4673-8851-1. doi: 10.1109/CVPR.2016.90.
- Hu, S., Fang, Z., An, H., Xu, G., Zhou, Y., Chen, X., and Fang, Y. Adaptive Communications in Collaborative Perception with Domain Alignment for Autonomous Driving, October 2023.
- Hu, S., Fang, Z., Deng, Y., Chen, X., and Fang, Y. Collaborative Perception for Connected and Autonomous Driving: Challenges, Possible Solutions and Opportunities, January 2024a.
- Hu, S., Fang, Z., Deng, Y., Chen, X., Fang, Y., and Kwong, S. Toward Full-Scene Domain Generalization in Multi-Agent Collaborative Bird’s Eye View Segmentation for Connected and Autonomous Driving. *IEEE Transactions on Intelligent Transportation Systems*, pp. 1–14, 2024b. ISSN 1558-0016. doi: 10.1109/TITS.2024.3506284.
- Hu, S., Fang, Z., Fang, Z., Deng, Y., Chen, X., and Fang, Y. AgentsCoDriver: Large Language Model Empowered Collaborative Driving with Lifelong Learning, April 2024c.
- Hu, S., Fang, Z., Fang, Z., Deng, Y., Chen, X., Fang, Y., and Kwong, S. AgentsCoMerge: Large Language Model Empowered Collaborative Decision Making for Ramp Merging, August 2024d.
- Hu, S., Tao, Y., Xu, G., Deng, Y., Chen, X., Fang, Y., and Kwong, S. CP-Guard: Malicious Agent Detection and Defense in Collaborative Bird’s Eye View Perception, 2024e.
- Hu, Y., Fang, S., Lei, Z., Zhong, Y., and Chen, S. Where2comm: Communication-efficient collaborative perception via spatial confidence maps. In *Proceedings*

- of the 36th International Conference on Neural Information Processing Systems, NIPS '22, pp. 4874–4886, Red Hook, NY, USA, April 2024f. Curran Associates Inc. ISBN 978-1-7138-7108-8.
- Kurakin, A., Goodfellow, I., and Bengio, S. Adversarial examples in the physical world, 2017.
- Li, Y., Ma, D., An, Z., Wang, Z., Zhong, Y., Chen, S., and Feng, C. V2X-Sim: Multi-Agent Collaborative Perception Dataset and Benchmark for Autonomous Driving. *IEEE Robotics and Automation Letters*, 7(4):10914–10921, October 2022. ISSN 2377-3766, 2377-3774. doi: 10.1109/LRA.2022.3192802.
- Li, Y., Fang, Q., Bai, J., Chen, S., Juefei-Xu, F., and Feng, C. Among Us: Adversarially Robust Collaborative Perception by Consensus. In *2023 IEEE/CVF International Conference on Computer Vision (ICCV)*, pp. 186–195, Paris, France, October 2023. IEEE. ISBN 979-8-3503-0718-4. doi: 10.1109/ICCV51070.2023.00024.
- Lin, Z., Qu, G., Chen, Q., Chen, X., Chen, Z., and Huang, K. Pushing large language models to the 6g edge: Vision, challenges, and opportunities. *arXiv preprint arXiv:2309.16739*, 2023.
- Lin, Z., Chen, Z., Fang, Z., Chen, X., Wang, X., and Gao, Y. FedSn: A federated learning framework over heterogeneous leo satellite networks. *IEEE Transactions on Mobile Computing*, 2024a.
- Lin, Z., Hu, X., Zhang, Y., Chen, Z., Fang, Z., Chen, X., Li, A., Vepakomma, P., and Gao, Y. Splitlora: A split parameter-efficient fine-tuning framework for large language models. *arXiv preprint arXiv:2407.00952*, 2024b.
- Lin, Z., Qu, G., Chen, X., and Huang, K. Split learning in 6g edge networks. *IEEE Wireless Communications*, 2024c.
- Lin, Z., Qu, G., Wei, W., Chen, X., and Leung, K. K. Adaptsfl: Adaptive split federated learning in resource-constrained edge networks. *arXiv preprint arXiv:2403.13101*, 2024d.
- Lin, Z., Wei, W., Chen, Z., Lam, C.-T., Chen, X., Gao, Y., and Luo, J. Hierarchical split federated learning: Convergence analysis and system optimization. *arXiv preprint arXiv:2412.07197*, 2024e.
- Lin, Z., Zhu, G., Deng, Y., Chen, X., Gao, Y., Huang, K., and Fang, Y. Efficient parallel split learning over resource-constrained wireless edge networks. *IEEE Transactions on Mobile Computing*, 2024f.
- Lin, Z., Zhang, Y., Chen, Z., Fang, Z., Wu, C., Chen, X., Gao, Y., and Luo, J. Leo-split: A semi-supervised split learning framework over leo satellite networks. *arXiv preprint arXiv:2501.01293*, 2025.
- Luo, W., Yang, B., and Urtasun, R. Fast and furious: Real time end-to-end 3d detection, tracking and motion forecasting with a single convolutional net. In *Proceedings of the IEEE Conference on Computer Vision and Pattern Recognition (CVPR)*, June 2018.
- Madry, A., Makelov, A., Schmidt, L., Tsipras, D., and Vladu, A. Towards deep learning models resistant to adversarial attacks. In *International Conference on Learning Representations*, 2018.
- Tao, Y., Hu, S., Fang, Z., and Fang, Y. Direct-CP: Directed Collaborative Perception for Connected and Autonomous Vehicles via Proactive Attention, 2024.
- Tao, Y., Hu, S., Hu, Y., An, H., Cao, H., and Fang, Y. GCP: Guarded Collaborative Perception with Spatial-Temporal Aware Malicious Agent Detection, 2025.
- Tu, J., Wang, T., Wang, J., Manivasagam, S., Ren, M., and Urtasun, R. Adversarial Attacks On Multi-Agent Communication. In *2021 IEEE/CVF International Conference on Computer Vision (ICCV)*, pp. 7748–7757, October 2021. doi: 10.1109/ICCV48922.2021.00767.
- Wang, T.-H., Manivasagam, S., Liang, M., Yang, B., Zeng, W., and Urtasun, R. V2VNet: Vehicle-to-Vehicle Communication for Joint Perception and Prediction. In Vedaldi, A., Bischof, H., Brox, T., and Frahm, J.-M. (eds.), *Computer Vision – ECCV 2020*, pp. 605–621, Cham, 2020. Springer International Publishing. ISBN 978-3-030-58536-5. doi: 10.1007/978-3-030-58536-5\_36.
- Xu, R., Xiang, H., Xia, X., Han, X., Li, J., and Ma, J. OPV2V: An Open Benchmark Dataset and Fusion Pipeline for Perception with Vehicle-to-Vehicle Communication. In *2022 International Conference on Robotics and Automation (ICRA)*, pp. 2583–2589, Philadelphia, PA, USA, May 2022. IEEE. ISBN 978-1-7281-9681-7. doi: 10.1109/ICRA46639.2022.9812038.
- Zhao, Y., Xiang, Z., Yin, S., Pang, X., Chen, S., and Wang, Y. Malicious Agent Detection for Robust Multi-Agent Collaborative Perception, July 2024.